XINN, Volume *1*

Supplemental Information

Daily CO_2 Emission Reduction Indicates the Control of Activities to Contain COVID-19 in China

Rong Wang, Yuankang Xiong, Xiaofan Xing, Ruipu Yang, Jiarong Li, Yijing Wang, Junji Cao, Yves Balkanski, Josep Peñuelas, Philippe Ciais, Didier Hauglustaine, Jordi Sardans, Jianmin Chen, Jianmin Ma, Tang Xu, Haidong Kan, Yan Zhang, Tomohiro Oda, Lidia Morawska, Renhe Zhang, and Shu Tao

Supplementary Methods

Monthly energy data by sector and province in China for 2016–2020

We compiled the annual data of energy consumption over the 21 years of 1997 to 2017 by selecting 30 provinces in China except for Tibet, Hong Kong, Macau and Taiwan due to lack of data. Following a method in the literature,[1] the consumption of coal, oil, and gas was collected for 14 sectors from the National Bureau of Statistics of China,[2] which was converted to energy in joules using a constant heat value for coal (0.015–0.026 TJ [t coal]$^{-1}$), oil (0.043–0.044 TJ [t oil]$^{-1}$), and gas (430–3890 TJ [10^8 m^3 gas]$^{-1}$).[1] Annual data of energy consumption over 1997–2017 in 14 sectors in 30 provinces are listed in **Supplementary Spreadsheet S1**.

To estimate the annual data of energy consumption by sector over 1997–2017 and the monthly data of energy consumption by sector over 2016–2020, the products produced or services supplied (see a list of these activities in **Table S2**) were compiled from the National Bureau of Statistics of China and the Ministry of Transport of the People's Republic of China.[3,4] Since the monthly activity data for January and February are given together, activities, energy consumption, and the corresponding CO_2 emissions in January and February were considered as a total.

Then, the energy consumption (J) was predicted by month based on the data of activity as:

$$J_{mths} = \sum_{z=1}^{n_s} \alpha_{hz} A_{mthz} + \beta_{hz} \quad (1)$$

where h is a province, s is a sector, m is a month, t is a year, z is one of the predictors (see **Table S2** for a list of predictors used to predict the energy consumption in 14 sectors), n_s is the number of predictors used to predict energy consumption in the sector, α_{hz} and β_{hz} are coefficients derived from regression models (see these coefficients in **Supplementary Spreadsheet S1**), and A_{mthz} is the activity of predictor z in month m. Although the relationship between energy consumption and activity may deviate from a linearity in extreme cases, we assumed that linear functions can be used when most changes in activities during COVID-19 are within the ranges observed in historical data over 1997–2017 as shown in **Supplementary Spreadsheet S1**.

For urban/rural residential energy usage and farming, forestry, animal husbandry, fishery, and water conservancy sectors, we developed 14×30=420 regression models between annual energy consumption and urban or rural population and predicted the annual energy consumption values for 2016–2020 by urban or rural population,[3] which were evenly allocated to 12 months. For wholesale, retail trade and catering services and other service sectors, the annual energy

consumption in the 5-year period of 2016–2020 was allocated to 12 months using the monthly distribution of production in China.[3]

In addition to the 14 sectors listed in **Table S2**, the remaining sectors contributing 4% of the total energy consumption in China were combined into one sector. For this sector, the annual energy consumption in 2010–2017 was regressed against year,[3] which was used to predict the annual energy consumption in 2018–2020. Then, the annual energy consumption was evenly allocated to 12 months.

For cement production, monthly activity data in January–May over 2016–2020 and in December over 2015–2019 were compiled from the National Bureau of Statistics of China.[3]

Daily NO_2 columnar concentration and meteorology

A daily data set of satellite-based NO_2 columnar concentration is retrieved from the backscattered radiance and solar irradiance at a wavelength of 270 to 500 nm with a spectral resolution of approximately 0.5 nm measured by a push broom ultraviolet-visible (UV-Vis) spectrometer in the Ozone Monitoring Instrument (OMI) on NASA's Aura satellite platform.[5] The daily measurement mode of OMI samples the swath width of 2600 km for the complete wavelength range with a nadir field-of-view (FOV) resolution of 13 km×24 km (along×across track), which has been shown to be stable with minimal degradation over the past 14 years.[6] For this study, we used the OMI global daily gridded NO_2 product version 3.0 (OMNO$_2$d: OMI/Aura NO_2 Cloud-Screened Total and Tropospheric Column L3 Global Gridded 0.25º×0.25º V3) from the Earth Observing System Data and Information System Distributed Active Archive Centers (https://earthdata.nasa.gov/).

Daily meteorological data were compiled from the Google Earth Engine cloud platform (https://developers.google.com/earth-engine/datasets/catalog). The data originate from three sources: 1) the relative humidity at 2 m above the ground, meridional wind at 10 m above the ground, zonal wind at 10 m above ground, columnar precipitable water content in the air, air temperature at 2 m above the ground, and surface wind speed at 10 m above the ground at a resolution of 0.25º×0.25º were generated by the Global Forecast System (GFS) operated by the National Center for Environmental Predictions (NCEP);[7] 2) the atmospheric pressure and planetary boundary layer height at a resolution of 0.2º×0.2º were generated by the Climate Forecast System (CFSv2) and Climate Forecast System Reanalysis (CFSR), respectively, operated by NCEP; [7] and 3) the ozone columnar concentration at a resolution of 0.01º×0.01º was measured by the Tropospheric Monitoring Instruments (TROPOMI) on the Sentinel-5 Precursor satellite.[7]

Average of NO_2 columnar concentration by region

Given the overlap of high CO_2 emissions and high pollutant concentrations in China, we calculated an average NO_2 columnar concentration weighted by CO_2 emissions in each province as:[8]

$$C_{hjt}=\frac{\sum_{i=1}^{n_h} C_{ijt}\cdot \overline{E_i^{detrended}}}{\sum_{i=1}^{n_h} \overline{E_i^{detrended}}} \quad (2)$$

where h is a province, i is a grid, j is a day, t is a year, n_h is number of grids in region h, $\overline{E_i^{detrended}}$ is the gridded CO_2 emission averaged in January–May 2016–2019.

To obtain $\overline{E}_i$, we mapped our bottom-up estimation of CO_2 emissions over January–May in 2016–2019 to a spatial resolution of 0.1°×0.1°, using a global monthly gridded dataset of CO_2 emission at a resolution of 0.1°×0.1° from the Open-source Data Inventory for Anthropogenic CO_2 (ODIAC) inventory developed by the Center for Global Environmental Research.[9] In this product, the authors have disaggregated national CO_2 emissions to 0.1°×0.1° grids using satellite-based observations of nightlight and global data sets of point sources.[10] For each grid, CO_2 emission rate in January–May over 2016–2019 is calculated as

$$E_{mti}^{detrended}=E_{mth}^{detrended}\frac{R_{mi}}{\sum_{i=1}^{n_h} R_{mi}},\ i\in h \quad (3)$$

where i is a grid, m is a month, t is a year, h is a province, R_{mi} is the gridded CO_2 emission from ODIAC averaged in January–May 2016–2018, n_h is the number of grids in province h, and $E_{mth}^{detrended}$ is the detrended CO_2 emissions in province h from our bottom-up estimate.

Artificial scenarios of daily CO_2 emissions in 2020

To estimate the public-health costs of CO_2 emissions, we estimated the costs of health care for cured cases and mortality costs for fatal cases during the COVID-19 pandemic. Considering the difference in the unit cost of a cured or fatal case, we divided the population into nine age groups (0-9, 10–19, 20–29, 30–39, 40–49, 50–59, 60–69, 70–79, and ≥80 years old). We calculated the health-care and mortality costs in January–May 2020 for each province as:

$$T_h=\sum_{d=1}^{152} dN_{dh}\cdot\left(cc_h\cdot\sum_{\eta=1}^{9}\sigma_\eta\cdot\Phi_{cc,\eta}+fc_h\cdot\sum_{\eta=1}^{9}\delta_\eta\cdot\Phi_{fc,\eta}\right) \quad (4)$$

where h is a province, d is a day, η is an age group, 152 denotes the day 31 May 2020, N_{hd} is the daily number of confirmed COVID-19 cases, cc_h or fc_h is the fraction of cured or fatal cases during COVID-19 in each province,[11] σ_η or δ_η is the fraction of an age group η in cured or fatal cases,[12]

$\Phi_{cc,\eta}$ is the unit cost in the course of infection for a cured case,[13] and $\Phi_{fc,\eta}$ is the unit cost in the course of infection for a fatal case.[14] We estimated the economic values of these avoided mortalities by dividing the deaths into nine age groups and applying the age-specified cost of premature mortality based on mortality risk valuation.[14]

To estimate the economic costs of health care and fatalities for COVID-19 cases associated with CO_2 emissions, we simulated the evolution of daily COVID-19 cases from 1 January to 31 May 2020 when one tonne of CO_2 was emitted by maintaining the CO_2-emitting activity on a given day in any province. We estimated the marginal costs (ξ_{jh}) as change in the costs (dT_h) when the CO_2 emissions on a given day j were changed from E_{jh} to (E_{jh}+dE_{jh}) in a given province as:

$$\xi_{jh} = \frac{dT_h}{dE_{jh}} \tag{5}$$

It should be noted change in CO_2 emissions on day j only affects the rate of new COVID-19 cases on these days after day j (N_{hd} with $d > j$), as is considered in our model.

To ensure the repeatability of calculation, the values of parameters for cc_h, fc_h, σ_η, δ_η, $\Phi_{cc,\eta}$ and $\Phi_{fc,\eta}$ are listed in **Tables S4, S5**. The data of CO_2 emission reduction due to COVID-19 from 1 January to 31 May (E_{jh}) were estimated by bottom-up or top-down methods (Figures 1,2 in the main text). The relationship between the daily number of new COVID-19 cases (N_{hd}) and the reduction of CO_2 emissions was described in the main text (Eqs. 10-13).

Finally, we calculated the marginal costs of health care and fatalities by maintaining CO_2-emitting activity (ξ_j) as an average of the marginal costs in 30 provinces (ξ_h) which are weighted by provincial CO_2 emission as:

$$\xi_j = \frac{\sum_{h=1}^{30} (\xi_{jh} \cdot \overline{E_{h,2016\text{-}2019}})}{\sum_{h=1}^{30} \overline{E_{h,2016\text{-}2019}}} \tag{6}$$

where j is a day, h is a province and $\overline{E_{h,2016\text{-}2019}}$ is the detrended CO_2 emission as an average for 2016–2019 in province h.

Supplementary Figures

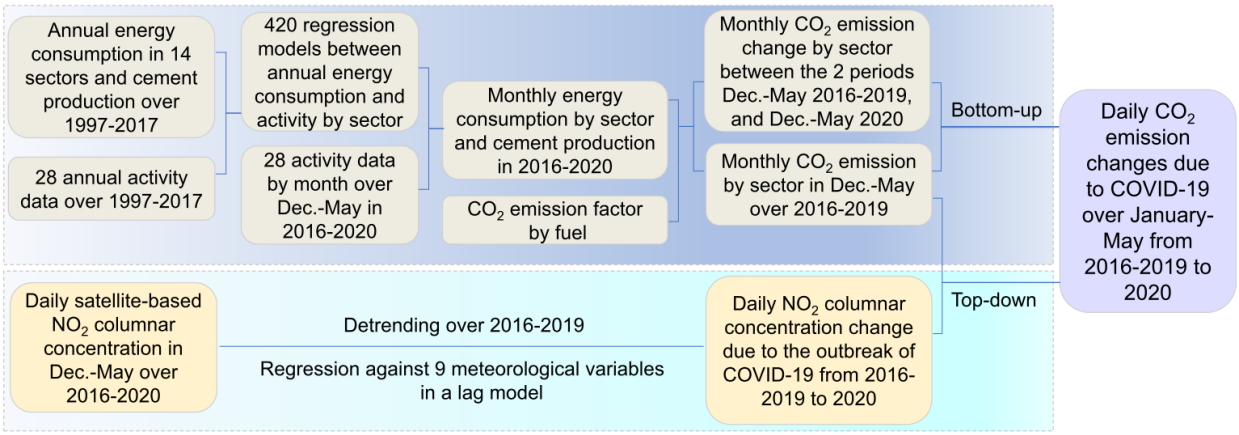

Figure S1. A scheme for estimating the impact of COVID-19 on daily CO_2 emissions with a top-down or bottom-up method.

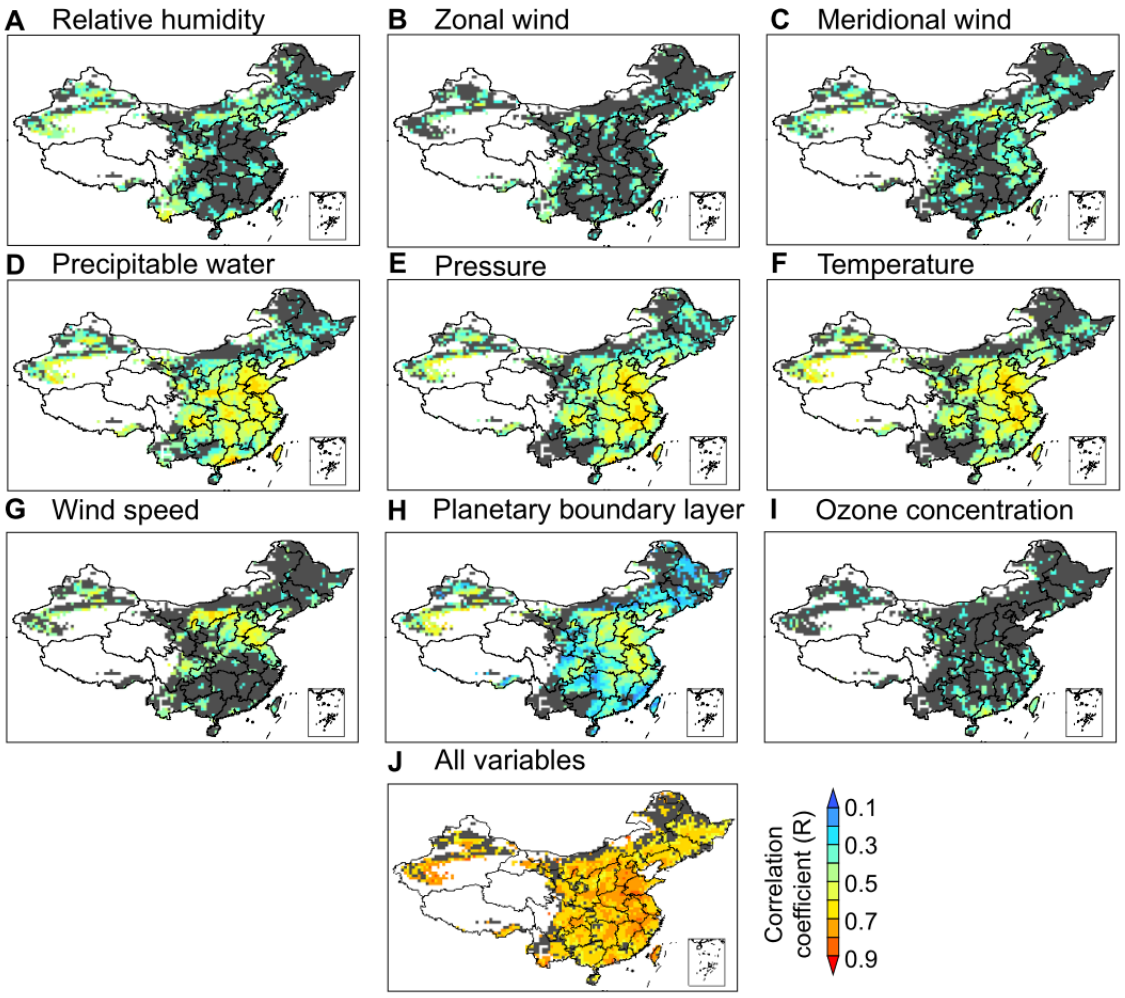

Figure S2. Correlation coefficients between NO_2 columnar concentration and nine meteorological variables.

Correlation coefficients are mapped for the $\log_{10}$-transformed daily NO_2 columnar concentrations against relative humidity at 2 m above the ground (**a**), zonal wind at 10 m above the ground (**b**), meridional wind at 10 m above ground (**c**), columnar precipitable water content in the air (**d**), atmospheric pressure at the ground (**e**), temperature at 2 m above the ground (**f**), surface wind speed at 10 m above the ground (**g**), planetary boundary layer height (**h**), ozone columnar concentration (**i**), and all variables (**j**). Grids with P>0.05 are marked in grey, while grids with missing data are shown in white.

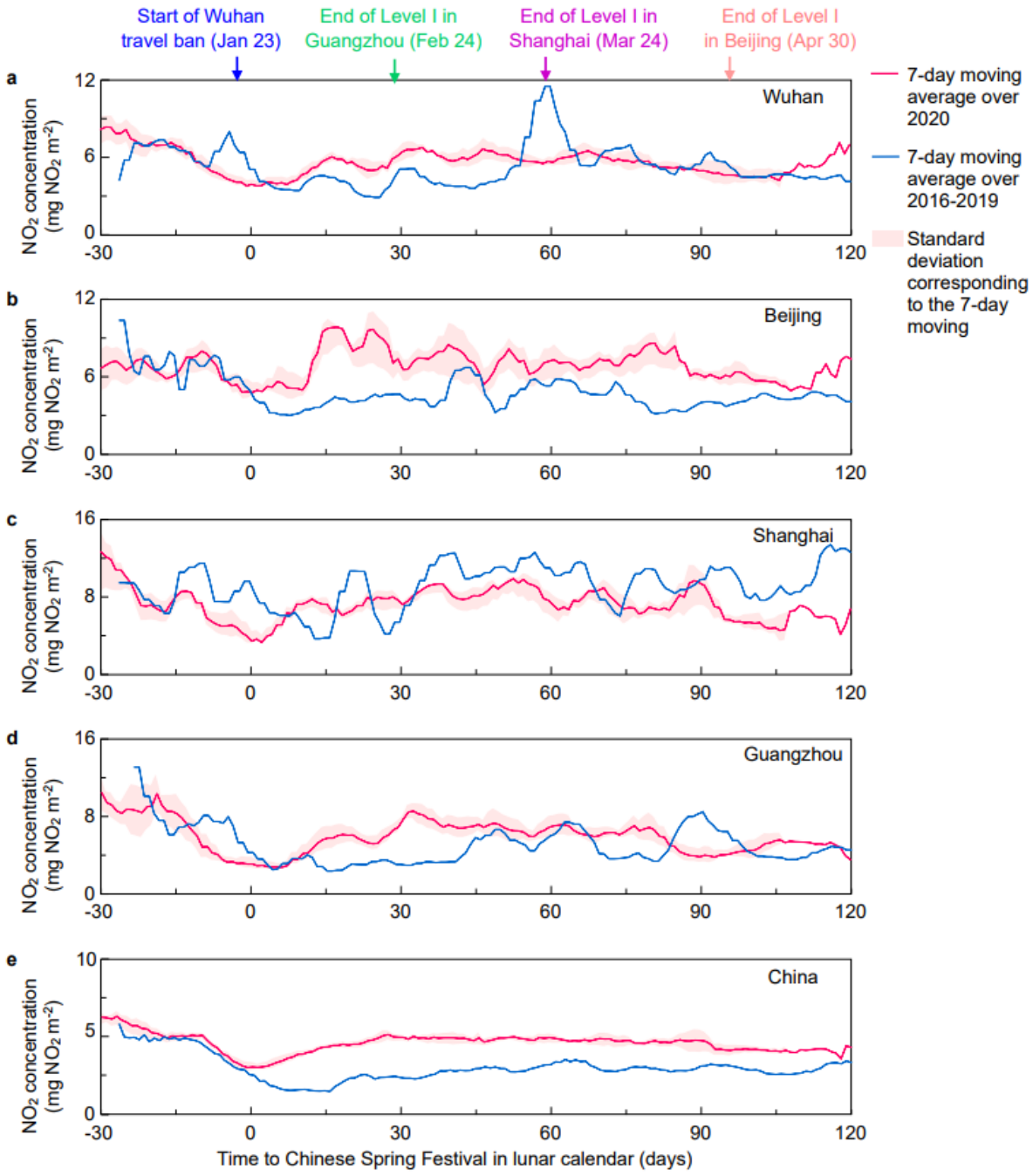

Figure S3. Comparison of NO_2 columnar concentration during the 150 days around Chinese New Year from 2016–2019 to 2020.

The concentration is shown as a 7-day moving average for a given day in 2020 and the same day in the lunar calendar in 2016–2019, which is used to compute the concentration confinement factor in Wuhan (**a**), Beijing (**b**), Shanghai (**c**), Guangzhou (**d**) and China (**e**). The standard deviation for the moving average in 2016–2019 is shown as the shaded area. The starting day of the Wuhan travel ban (23 January) and the end day of the Level I emergency response in Guangzhou (24 February), Shanghai (24 March) and Beijing (30 April) in 2020 are marked by arrows.

Supplementary Tables

Table S1. Comparison of concentration confinement factor and emission confinement factor by province.

To compare the satellite-based NO_2 columnar concentration changes with the activity-based CO_2 emission reduction, we computed an emission confinement factor (ECF) and a concentration confinement factor (CCF) (see Eqs. 1,2 in the main text) as the ratio of NO_2 columnar concentration and CO_2 emissions between January and May in 2020 and the same period over 2016–2019. The values of CCF and ECF are given by province for Jan–May.

Province	CCF				ECF			
	Jan-Feb	Mar	Apr	May	Jan-Feb	Mar	Apr	May
Beijing	0.72	0.71	0.61	0.82	0.91	0.95	1.02	0.98
Tianjin	0.70	0.58	0.58	0.70	0.76	0.72	0.76	0.75
Hebei	0.68	0.64	0.66	0.68	0.92	0.96	0.91	0.91
Shanxi	0.65	0.68	0.59	0.65	0.95	1.07	1.14	1.12
Inner Mongolia	0.83	0.85	0.80	0.82	0.88	0.83	0.91	0.89
Liaoning	0.84	0.78	0.80	0.73	0.91	0.88	0.90	0.96
Jilin	0.90	0.78	0.91	0.75	0.94	0.89	0.92	0.95
Heilongjiang	0.76	0.64	0.73	0.64	0.82	0.88	0.87	0.84
Shanghai	0.74	0.88	0.92	1.05	0.81	0.79	0.85	0.89
Jiangsu	0.71	0.71	0.83	0.82	0.75	0.83	1.01	1.06
Zhejiang	0.71	0.91	0.92	0.90	0.70	0.84	0.86	0.98
Anhui	0.62	0.63	0.70	0.71	0.85	0.96	0.98	0.99
Fujian	0.74	0.73	0.72	0.67	0.77	0.94	0.86	0.87
Jiangxi	0.65	0.68	0.67	0.82	0.78	0.88	0.91	1.01
Shandong	0.60	0.54	0.59	0.65	0.89	1.03	0.98	0.96
Henan	0.63	0.68	0.76	0.72	0.88	1.02	1.03	1.09
Hubei	0.74	0.75	0.95	0.99	0.67	0.61	0.77	0.86
Hunan	0.67	0.65	0.71	0.87	0.91	1.07	1.11	1.21
Guangdong	0.67	0.66	0.76	0.65	0.81	0.90	0.96	1.09
Guangxi	0.83	0.86	0.95	0.81	1.01	1.06	1.12	1.07
Hainan	0.90	0.93	0.92	0.93	0.82	0.84	0.85	0.99
Chongqing	0.68	0.68	0.71	0.65	0.75	0.87	0.93	1.01
Sichuan	0.76	0.71	0.75	0.74	0.86	0.88	0.95	1.01
Guizhou	0.72	0.72	0.79	0.64	0.73	0.77	0.89	0.95
Yunnan	0.74	0.98	0.98	0.82	0.75	0.89	0.90	0.92
Shaanxi	0.74	0.83	0.72	0.87	0.85	0.84	0.86	0.90
Gansu	0.86	0.96	0.90	0.95	0.85	0.85	1.01	1.10
Qinghai	0.90	0.99	1.02	1.06	0.83	1.01	1.09	1.03
Ningxia	0.90	0.97	0.85	1.00	0.85	0.88	1.04	1.02

Xinjiang	0.73	0.69	0.78	0.75	0.93	0.89	1.03	0.95

Table S2. Activity data used to predict the monthly energy consumption.

A total of 28 types of activity data were used to predict the monthly energy consumption in 14 sectors by 420 regression models for 30 provinces. The number of activity data items used to predict the energy consumption in each sector, equal to the number of independent variables in the regression model by sector, is given in parenthesis.

#	Sector name	Activity data
1	Production and supply of electric power, steam and hot water	Thermal power generation (1)
2	Smelting and pressing of ferrous metals	Pig iron production, and steel production (2)
3	Non-metal mineral products	Cement production (1)
4	Transportation, storage, post and telecommunication services	Passenger turnover, cargo turnover, and express delivery number (3)
5	Urban residential energy usage	Urban population (1)
6	Coal mining and dressing	Raw coal production (1)
7	Petroleum processing and coking	Gasoline, kerosene, diesel, energy oil, and coke production (5)
8	Rural residential energy usage	Rural population (1)
9	Wholesale, retail trade and catering services	Total retail sales of social consumer goods (1)
10	Other service sectors	Total retail sales of social consumer goods (1)
11	Raw chemical materials and chemical products	Sulfuric acid, Caustic soda, fertilizer, plastic, and fiber production (5)
12	Farming, forestry, animal husbandry, fishery and water conservancy	Gross output value of agriculture, forestry, animal husbandry and fishery (4)
13	Smelting and pressing of nonferrous metals	Production of ten non-ferrous metals (1)
14	Construction	New construction area of real estate (1)

Table S3. Coefficients in the regression of daily rate of COVID-19 cases against the CO_2 emission reduction by province.

The slope, intercept, and square of Pearson's correlation coefficient (R^2), and the *p*-value of linear regression between the daily rate of new COVID-19 cases and the total CO_2 emission reduction estimated using a bottom-up or top-down method are given by province.

Province	Bottom-up method				Top-down method			
	Slope	Intercept	R^2	*p*-value	Slope	Intercept	R^2	*p*-value
Beijing	-7.46	0.16	0.75	<0.001	-5.57	0.16	0.74	<0.001
Tianjin	-3.72	0.13	0.22	0.01	-3.57	0.13	0.22	0.01
Hebei	-10.51	0.25	0.57	<0.001	-7.69	0.28	0.57	<0.001
Shanxi	-9.86	0.13	0.82	<0.001	-6.88	0.18	0.81	<0.001
Inner-Mongolia	-3.11	0.08	0.08	0.38	-3.03	0.08	0.08	0.39
Liaoning	-7.3	0.09	0.2	0.13	-7.06	0.09	0.21	0.11
Jilin	-7.13	0.08	0.21	0.18	-7.13	0.08	0.21	0.18
Heilongjiang	-7.74	0.3	0.66	<0.001	-7.72	0.3	0.66	<0.001
Shanghai	-6.89	0.12	0.56	<0.001	-6.49	0.12	0.57	<0.001
Jiangsu	-9.77	0.26	0.82	<0.001	-9.56	0.26	0.82	<0.001
Zhejiang	-9.31	0.2	0.54	<0.001	-10.35	0.19	0.53	<0.001
Anhui	-12.47	0.35	0.91	<0.001	-9.52	0.37	0.92	<0.001
Fujian	-11.54	0.23	0.66	<0.001	-12.11	0.23	0.66	<0.001
Jiangxi	-15.46	0.32	0.84	<0.001	-13.37	0.35	0.86	<0.001
Shandong	-2.2	0.02	0.03	0.42	-1.22	0	0.02	0.53
Henan	-7.97	0.18	0.73	<0.001	-6.08	0.2	0.74	<0.001
Hubei	-4.57	0.25	0.76	<0.001	-5.7	0.24	0.75	<0.001
Hunan	-8.8	0.14	0.49	<0.001	-7.39	0.16	0.51	<0.001
Guangdong	-9.29	0.16	0.5	<0.001	-8.05	0.18	0.52	<0.001
Guangxi	-23.92	0.02	0.21	0.09	-13.23	0.04	0.27	0.05
Hainan	-9.25	0.05	0.17	0.12	-17.14	0.05	0.22	0.06
Chongqing	-4.06	0.1	0.46	<0.001	-3.86	0.1	0.46	<0.001
Sichuan	-9.53	0.22	0.69	<0.001	-7.71	0.22	0.68	<0.001
Guizhou	-14.6	0.43	0.63	0.001	-15.42	0.43	0.64	0.001
Yunnan	-5.11	0.08	0.14	0.11	-5.43	0.08	0.14	0.11
Shaanxi	-15.55	0.26	0.76	<0.001	-13.07	0.28	0.77	<0.001
Gansu	-1.84	0.04	0.01	0.7	-2.37	0.04	0.01	0.7
Ningxia	-14.9	0.27	0.51	0.07	-17.96	0.26	0.51	0.07
Xinjiang	-7.02	0.15	0.4	0.003	-4.15	0.16	0.38	0.004

Table S4. The fraction of cured and fatal cases by province.

Province	Fraction of cured cases (%) (RRTD, 2020)[11]	Fraction of fatal cases (%)
Beijing	98.99	1.01
Tianjin	98.48	1.52
Hebei	98.28	1.72
Shanxi	100	0
Inner-Mongolia	99.58	0.42
Liaoning	98.7	1.3
Jilin	98.71	1.29
Heilongjiang	98.63	1.37
Shanghai	99.01	0.99
Jiangsu	100	0
Zhejiang	99.92	0.08
Anhui	99.39	0.61
Fujian	99.72	0.28
Jiangxi	99.89	0.11
Shandong	99.12	0.88
Henan	98.28	1.72
Hubei	93.38	6.62
Hunan	99.61	0.39
Guangdong	99.51	0.49
Guangxi	99.21	0.79
Hainan	96.49	3.51
Chongqing	98.97	1.03
Sichuan	99.49	0.51
Guizhou	98.64	1.36
Yunnan	98.92	1.08
Shaanxi	99.06	0.94
Gansu	98.77	1.23
Qinghai	100	0
Ningxia	100	0
Xinjiang	96.05	3.95

Table S5. Age distribution and unit cost for a cured or fatal case.

The population was divided into nine age groups. The age distribution and unit cost in the course of infection for a cured or fatal case were applied for each group. The uncertainties as a percentage of the 95% confidence interval to the central value in the unit costs are given in parentheses, and are applied in our Monte Carlo simulations.

Age group	Fraction of age group in cured cases (%)	Fraction of age group in fatal cases (%)	Cost for a cured case (thousand 2020 $)	Cost for a fatal case (million 2020 $)
	Novel, 2020[12]	Novel, 2020[12]	Bartsch et al, 2020[13]	Thunström et al, 2020[14]
0–9	0.90	0.00	14.7 (±3%)	14.7 (±3%)
10–19	1.20	0.10	14.7 (±3%)	15.3 (±3%)
20–29	8.10	0.70	17.0 (±3%)	16.1 (±3%)
30–39	17.00	1.80	17.0 (±3%)	15.8 (±3%)
40–49	19.20	3.70	20.6 (±3%)	13.8 (±3%)
50–59	22.40	12.70	20.6 (±3%)	10.3 (±3%)
60–69	19.20	30.20	19.2 (±3%)	6.7 (±3%)
70–79	8.80	30.50	19.2 (±3%)	3.7 (±3%)
≥80	3.20	20.30	15.4 (±3%)	1.5 (±3%)

References

1. Shan, Y., Huang, Q., Guan, D., et al. (2020). China CO_2 emission accounts 2016–2017. Sci. Data 7, 1-9.
2. National Bureau of Statistics of China (NBSC). (2018). China Energy Statistics Yearbook. http://www.stats.gov.cn/english/Statisticaldata/AnnualData/.
3. National Bureau of Statistics of China (NBSC). (2020). Statistical Database. http://www.stats.gov.cn/english/Statisticaldata/AnnualData/.
4. Ministry of Transport of the People's Republic of China (MTPRC). (2020). Statistical Database. http://www.mot.gov.cn/.
5. Krotkov, N.A., Lamsal, L.N., Celarier, E.A., et al. (2017). The version 3 OMI NO_2 standard product. Atmos. Meas. Tech. 10, 3133-3149.
6. Levelt, P.F., Joiner, J., Tamminen, J., et al. (2018). The Ozone Monitoring Instrument: overview of 14 years in space. Atmos. Chem. Phys. 18, 5699-5745.
7. Gorelick, N., Hancher, M., Dixon, M., et al. (2017). Google Earth Engine: Planetary-scale geospatial analysis for everyone. Remote Sens. Environ. 202, 18-27.
8. Wang, R., Tao, S., Balkanski, Y., et al. (2014). Exposure to ambient black carbon derived from a unique inventory and high-resolution model. Proc. Natl. Acad. Sci. USA. 111, 2459-2463.
9. Center for Global Environmental Research (CGER). (2020). ODIAC Fossil Fuel Emission Dataset. http://db.cger.nies.go.jp/dataset/ODIAC/.
10. Oda, T., Maksyutov, S., Andres, R.J. (2018). The Open-source Data Inventory for Anthropogenic Carbon dioxide (CO_2), version 2016 (ODIAC2016): A global, monthly fossil-fuel CO_2 gridded emission data product for tracer transport simulations and surface flux inversions. Earth Syst. Sci. Data 10, 87–107.
11. Report of Real Time Data of COVID-19 (RRTD). (2020). https://voice.baidu.com/act/newpneumonia/newpneumonia/?from=osari_pc_3.
12. Novel, C.P.E.R.E. (2020). The epidemiological characteristics of an outbreak of 2019 novel coronavirus diseases (COVID-19) — China, 2020. China CDC Weekly 2, 113-122.
13. Bartsch, S.M., Ferguson, M.C., McKinnell, J.A., et al. (2020). The potential health care costs and resource use associated with COVID-19 in the United States. Health Aff. 39, 927-935.

14. Thunström, L., Newbold, S.C., Finnoff, D., et al. (2020). The benefits and costs of using social distancing to flatten the curve for COVID-19. J. Benefit Cost Anal. 11, 179-195.